Quadrupolar perturbed ^{14}N NMR in the structurally commensurate and incommensurate phases of ammonium tetrachlorozincate

D. Michel,* B. Müller, J. Petersson, A. Trampert, and R. Walisch
Fachbereich Physik, Universität des Saarlandes, D-6600 Saarbrücken, Federal Republic of Germany
(Received 15 August 1990)

Quadrupolar perturbed ^{14}N NMR spectra were studied in the normal, incommensurate and the various commensurate phases of ammonium tetrachlorozincate $(NH_4)_2ZnCl_4$ (AZC) single crystals, in order to investigate local phenomena related to structural phase transitions. In the high-temperature normal and the commensurate lock-in phase, whose lattice constant is quadrupled along the c direction of the high-temperature structure, the electric-field-gradient (EFG) tensors at the nitrogen sites are determined by the well-known Volkoff formalism. The results are related to the symmetries of these phases. In particular, the space group of the commensurate phase mentioned could be derived, and the distinct influence of the domain structure is seen in the NMR spectra of that phase. The frequency distributions appearing in the incommensurate (IC) phase were studied as a function of both crystal orientation and temperature. The degeneracies and symmetries of the NMR rotation patterns in the incommensurate phase are discussed on the basis of the general symmetry properties of that phase, derived by a symmetry analysis of the phase sequence of AZC. The superspace group of the *IC* phase is equal to that determined for other A_2BX_4-type crystals like Rb_2ZnBr_4 and Rb_2ZnCl_4. The data can be fitted quantitatively by taking into account the nonvanishing terms of the lowest order in a general symmetry-adapted Fourier series for the EFG tensor. The temperature dependences of the NMR spectra observed in the incommensurate phase are related to the static critical behavior. It is in particular demonstrated that AZC and the other substances of the A_2BX_4-type mentioned show a universal static critical behavior.

I. INTRODUCTION

In some crystals of the A_2BX_4 type like, e.g., the isomorphous K_2SeO_4, Rb_2ZnBr_4, and Rb_2ZnCl_4—the latter are henceforth abbreviated as RZB and RZC, respectively—second-order phase transitions from a paraelectric normal (N) phase to an incommensurate (IC) phase occur at a temperature T_i. At a lower temperature T_c, there is a lock-in transition to a ferroelectric commensurate (C) phase whose unit cell is tripled along the c direction of the high-temperature structure. Ammonium tetrachlorozincate $(NH_4)_2ZnCl_4$, abbreviated as AZC, belongs to this class of substances, too. In the high-temperature normal phase ($T \geq T_i \approx 133\,^{\circ}C$),[1] an orthorhombic pseudohexagonal structure exists, and below about $-5\,^{\circ}C$, a ferroelectric $3C$ phase is present whose structure is isomorphous to that of the other substances mentioned. The phase sequence of AZC, however, is considerably different: At $T_1 = T_i \approx 133\,^{\circ}C$, a transition to an IC phase occurs[2] which is modulated along the c direction with a wave number close to $\frac{1}{4}$, contrasting to a value close to $\frac{1}{3}$ which is typical for the other substances. Correspondingly, at $T_2 = T_c \approx 91\,^{\circ}C$, the modulation locks in at a wave number $\frac{1}{4}$ thus giving rise to a commensurate $4C$ phase below T_c whose lattice constant is quadrupled along the c direction. In some experiments at $T_3 \approx 46\,^{\circ}C$, both structural and dielectric anomalies were reported, which sometimes were ascribed to another structural phase transition whose nature is still not clear. These anomalies are not the subject of the present work. In another publication[3] dealing with the dielectric behavior of AZC in a general context, the circumstances which cause these anomalies to appear are discussed. Between $T_4 \approx 0\,^{\circ}C$ and $T_5 \approx -5\,^{\circ}C$, a narrow weakly ferroelectric $\frac{7}{2}C$ phase with a wave number $\frac{2}{7}$ occurs, and below $-5\,^{\circ}C$ the ferroelectric $3C$ phase is present. Clearly, a special interest in AZC is established by these facts.

It is, therefore, surprising that, in comparison with the other substances of the A_2BX_4 type mentioned, only few experimental investigations on AZC exist. This situation seems to be related to the difficulties in growing crystals of sufficient quality. Since AZC starts to decompose at temperatures near the *N-IC* transition, single crystals cannot be grown from the melt. The special requirements to be fulfilled for crystal growth from aqueous solutions will be discussed below in Sec. II.

It was shown in many works that quadrupolar perturbed nuclear magnetic resonance (NMR) and nuclear quadrupole resonance (NQR) can contribute considerably to the understanding of the C and IC phases in the A_2BX_4 compounds. Nevertheless, NMR and NQR investigations near and around the incommensurate phase of AZC are not yet available in the literature. In previous works[4–6] the ^{35}Cl NQR spectra were studied near the ferroelectric phase transition of AZC ($-5\,^{\circ}C$). Although a temperature range between -123 and $47\,^{\circ}C$ was available, properties of the $3C$-$\frac{7}{2}C$-$4C$ phase sequence could not be monitored. ^1H NMR relaxation studies on AZC (Refs. 7 and 8) were mainly used to investigate dynamical processes at lower temperatures, also including, in particular, tunneling processes at very low temperatures.[9,10]

One of the main purposes of the present work is to overcome these shortcomings and to demonstrate that ^{14}N ($I=1$) quadrupolar perturbed NMR is a sensitive method for probing local structural properties in the various C and IC phases of AZC. Thus, it will be shown that, with respect to NMR, the situation very much resembles that of the ^{87}Rb nucleus in RZB and RZC (for more particulars see Refs. 11–13 and works cited within).

In the experiments being presented, the electric-field-gradient (EFG) tensor at the site of the ^{14}N nucleus is the physical quantity measured by quadrupolar perturbed NMR. The ^{14}N NMR spectrum consists of pairs of lines at frequencies $\nu_{\pm}$ corresponding to the transitions $m=\pm1\leftrightarrow m=0$. The distance $\nu_+-\nu_-$ is related to the EFG by a pure first-order effect in a perturbation-theory approach, taking into account terms up to second order, and is simply proportional to the component of the EFG in the direction of the static magnetic field $\mathbf{B}_0$.

Other substances which belong to this class of crystals and which were investigated by different experimental methods are tetramethylammonium tetrachlorozincate $[N(CH_3)_4]_2ZnCl_4$ (TMATC-Zn) and its isomorphs. Quadrupolar perturbed ^{14}N NMR spectra were also used for studying the static properties of the various C and IC phases in this substance.[14] Starting from a high-temperature N phase, which is isomorphous to the N phases of the other A_2BX_4 compounds discussed here, this crystal undergoes quite a different phase sequence. Thus, from a physical point of view, AZC may be assumed to form a link between the classical substances K_2SeO_4, RZB, and RZC on the one hand and TMATC-Zn on the other.

Recently a general formalism was established for describing and characterizing quadrupolar perturbed NMR spectra in both structurally commensurate and incommensurate phases in terms of structural parameters.[11] The method is based on the superspace formalism and on the use of modulation functions defined along a suitably defined internal space. This general approach was applied first to the interpretation of the ^{87}Rb NMR satellite transitions in RZB (Ref. 12) and more recently in RZC.[13] Another main purpose of the present work is to show that the results of static ^{14}N NMR measurements on AZC crystals can be treated in the same way, i.e., in terms of the symmetries of the various phases. In particular, the superspace symmetry of the IC phase is taken into account, which is equal to that determined for K_2SeO_4,[15], RZB,[12] and RZC.[13] By that means, a further proof will be given for the applicability of the general formalism to systems undergoing a more complicated phase sequence than those discussed so far. It will be demonstrated, in particular, that as in the other substances, so-called nonlocal effects must be taken into account for describing the ^{14}N spectra in the IC phase of AZC. Moreover, it will be shown that the critical exponents near the N-IC transition, as derived from the NMR results, can be well described by the general arguments introduced quite recently and so far, only applied to ^{87}Rb NMR in RZC.[13]

The paper is organized as follows: In Sec. II, experimental details with respect to crystal growth and the performance of the NMR measurements are described. In Sec. III, the experimental results are presented including the dependence of the ^{14}N NMR spectra on the rotation of the crystal around different crystallographic axes at various temperatures, viz., in the normal phase at 137 °C, in the commensurate $4C$ phase at 5 °C, and in the incommensurate phase at 108 °C. Moreover, the temperature dependence of the spectra is measured for special orientations between −20 and about +140 °C, which enables not only a proof of the assignment of the lines to certain nitrogen sites but also the determination of critical exponents in the IC phase. From the orientational dependence of the spectra in the IC phase, the EFG-modulation tensor functions will be derived (Sec. IV). The treatment is based on a symmetry analysis of the phase sequence N-IC-$4C$-$\frac{7}{2}C$-$3C$ of AZC.

II. EXPERIMENTAL DETAILS

Usually single crystals of A_2BX_4-type compounds are grown either from the melt or from aqueous solutions. Since AZC starts to decompose at temperatures near the N-IC transition, single crystals cannot be grown from the melt. Therefore, single crystals of AZC were grown from aqueous solutions of NH_4Cl and $ZnCl_2$. Meerburg[16] was the first to establish a detailed phase diagram of the system NH_4Cl, $ZnCl_2$, and water; according to the phase diagram a mixture of AZC and other compounds is generally obtained if, as usual, the solution contains the solvents with the stoichiometric ratio of 2:1. On the contrary, following Meerburg[16] we used aqueous solutions of the composition 1:1 at temperatures between 30 and 40 °C. By slowly lowering the temperature (initially about $\frac{1}{200}$ K and finally $\frac{1}{10}$ K per day), high-quality single crystals of AZC were grown with a size of about 1 cm^3. The time necessary for growing one crystal was between 2 and 3 months. All crystals were clear and transparent and had a direction of preferential growth along the b axis. The size of the samples used in the NMR experiments was about 15 mm and 5 mm along and perpendicular to the b axis, respectively. They were orientated by goniometric methods.

The ^{14}N NMR spectra were measured with a Brucker CXP-300 spectrometer operating at a static magnetic field of about 7 T. Single-pulse excitation with a pulse length of 6–7 μs was used, ensuring a nearly uniform excitation in the spectra which have a line splitting not exceeding 120 kHz. Note that the duration of the $\pi/2$ pulse was about 18 μs. The NMR sensitivity of the ^{14}N nuclei (10^{-3}) given at a constant field relative to an equal number of protons is small as compared to that of the ^{87}Rb nucleus (≈0.175) which, recently, was employed for investigating the IC phases in RZB (Ref. 12) and RZC.[13,17] Nevertheless, the use of ^{14}N NMR for studying AZC is still advantageous, in particular, in the IC phase near the lock-in transition because of the considerably narrower ^{14}N NMR spectra. Usually 50–100 scans with a repetition time of 5 s were taken to ensure sufficient spectral intensities, particularly in the IC phase. Depending on temperature, the longitudinal spin-

relaxation times varied between about 2 s and more than 20 s.[18] A special apparatus was available[17] which rendered it possible to rotate the crystal sample around an axis perpendicular to the static magnetic field $\mathbf{B}_0$ and to incline the probe head by small angles with respect to the axis of the cryomagnet. Thus, the orientation of the sample could be adjusted very accurately. Since the NMR spectra depend sensitively on the crystal orientation, this is an important condition to be obeyed.

A standard gas-flow temperature regulation was used, with a temperature stability of about ± 0.1 K over the measuring period. Special care was taken to reduce the temperature gradient over the sample volume to a value less than 0.3 K. This was particularly necessary on running the ^{14}N NMR measurements near the *N-IC* transition.

III. EXPERIMENTAL RESULTS

A. Crystal rotations in the normal phase

Defining the crystal axes $\mathbf{a}=a\mathbf{e}_x$, $\mathbf{b}=b\mathbf{e}_y$, and $\mathbf{c}=c\mathbf{e}_z$ in such a way that $a>c>b$ holds for the lattice constants where $a=12.745$ Å, $b=7.275$ Å, $c=9.295$ Å at 140 °C (Ref. 19), the space group *Pcmn* of the *N* phase is the same as that of other A_2BX_4 compounds, for instance, RZB,[12] RZC,[17] and K_2SeO_4.[15] Each unit cell contains four formula units and, hence, eight nitrogen atoms. There are two different kinds of ^{14}N nuclei, termed N(1) and N(2). The four ^{14}N nuclei of one particular kind are related to each other by symmetry relations leading to restrictions of the components V_{ij} of the EFG tensor at the N site. Values V_{xz} of equal magnitude but different sign belong to N nuclei which are related to each other by the glide planes c_x perpendicular to the *a* axis (glide vector: $\{0,0,c/2\}$) or by the glide planes n_z perpendicular to the *c* axis (glide vector: $\{a/2,b/2,0\}$). Since all N nuclei are placed in the mirror planes m_y perpendicular to the *b* axis, the tensor components V_{xy} and V_{yz} vanish. Thus, one principal axis of the EFG tensor is directed along the *b* axis. Consequently, also taking into account the Laplace equation $V_{xx}+V_{yy}+V_{zz}=0$, the complete EFG tensor can be determined from the dependence of the spectra on the rotation of the crystal around the *b* axis which is perpendicular to the direction of the constant external magnetic field $\mathbf{B}_0$ (*b* rotation) and by applying the well-known Volkoff formalism.[20] For the first-order splitting $\Delta\nu=\nu_+-\nu_-$, one obtains, for a *b* rotation,

$$\Delta\nu_y=\Phi_{zz}\cos^2\Theta_y+\Phi_{xx}\sin^2\Theta_y-\Phi_{xz}\sin 2\Theta_y\ , \qquad (1)$$

where $\Theta_y=\angle(\mathbf{c},\mathbf{B}_0)$, $\Phi_{ij}=(3eQ/2h)V_{ij}$ (for $I=1$), and $V_{ij}=\partial^2V/\partial x_i\partial x_j$. The corresponding relations for the other crystal rotations are obtained by cyclic permutation. As usual, we denote by V_{ij} and Φ_{ij} an element of the EFG tensor and the quadrupole coupling tensors, respectively, and by eQ the quadrupole moment of the ^{14}N nucleus. Defining the sign of the main diagonal element with the largest modulus to be positive, from the experimental data shown in Fig. 1, the following components Φ_{ij} (in units of kHz, $T=137$ °C) result: $\Phi_{xx}(1)=-5.6$, $\Phi_{yy}(1)=105.5$, $\Phi_{zz}(1)=-99.9$, $\Phi_{xz}(1)=\pm 18.5$ for N(1) and $\Phi_{xx}(2)=48.1$, $\Phi_{yy}(2)=-26.2$, $\Phi_{zz}(2)=-21.9$, $\Phi_{xz}(2)=\pm 2.1$ for N(2).

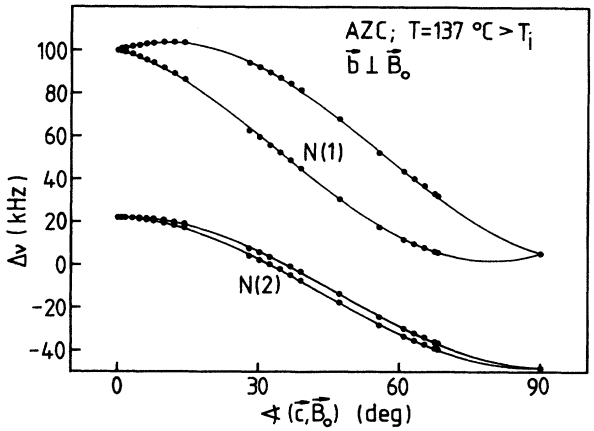

FIG. 1. Rotation pattern of the ^{14}N NMR line splittings $\Delta\nu=\nu_+-\nu_-$ in the *N* phase of AZC at about 137 °C for the orientation $\mathbf{b}\perp\mathbf{B}_0$. Fit curves according to Eq. (1).

From these values the angles Θ_y between the principal directions of the EFG lying in the mirror planes m_y and the crystallographic *a* and *c* axes can be readily derived as $\Theta_y=\pm 10.7°$ and $\pm 1.7°$ for N(1) and N(2), respectively. Transforming the principal-axes reference frame of the EFG tensor, one gets the field gradients $eq=105.5$; 48.2 kHz and the asymmetry parameters $\eta=0.96$, 0.087 for N(1) and N(2), respectively. Thus, the EFG at the N(2) site is nearly axially symmetric whereas it strongly deviates from axial symmetry at the N(1) site.

The values obtained from the *b* rotation are consistent with the *c*-rotation pattern of the ^{14}N NMR line splittings shown in Fig. 2. This provides an additional proof for the validity of the symmetry of the *N* phase given above. The orientations of the principal EFG tensor axes at both ^{14}N nuclei are approximately the same as those at

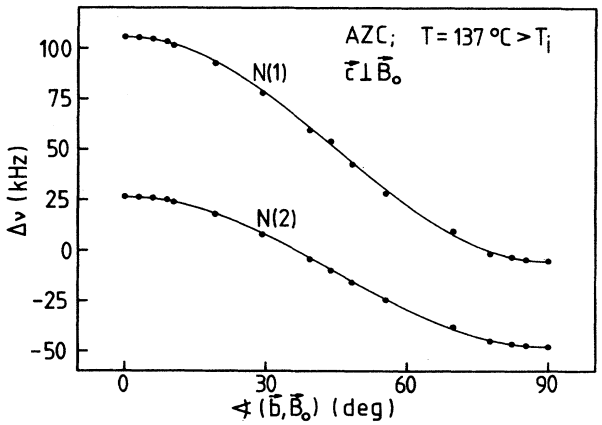

FIG. 2. Rotation pattern as in Fig. 1 for the orientation $\mathbf{c}\perp\mathbf{B}_0$. In order to achieve a more appropriate representation, different signs have been ascribed to the splitting of N(1) in Figs. 1 and 2.

the Rb sites in RZB (Ref. 12) and RZC.[17] The principal values, however, differ by more than 1 order of magnitude.

B. Crystal rotations in the commensurate 4C phase

In the 4C phase, the unit cell is quadrupled along the c direction of the N phase structure. Thus, the unit cell of the 4C phase contains 32 nitrogen nuclei. If the space group $P1c1$ proposed previously[19] is applied, the local surroundings of every two suitable nuclei are related to each other by the only symmetry operation c_y. Thus, 16 inequivalent ^{14}N nuclei are to be expected. Rotation patterns in the 4C phase principally make it possible to check whether or not this space group is in accordance with the symmetries of the ^{14}N NMR spectra. For that purpose a-, b-, and c-rotation patterns were taken at about 5 °C with angle variations between 0° and 180° in steps of 1.5° (b rotation) and 3° (a and c rotations).[21] According to the space group mentioned, twofold degenerate, i.e., 16, ^{14}N NMR line pairs would result for the b rotation and all orientations for which one of the crystallographic axes is parallel to the direction of the static magnetic field $\mathbf{B}_0$. In all other orientations, 32 line pairs are expected.

Comparing the results depicted in Figs. 3 and 4 for b and c rotations, respectively, to those presented in Figs. 1 and 2, the strong influence of the N-IC-4C transition sequence on the ^{14}N NMR spectra is clearly demonstrated (similar results are obtained for the a rotation not presented here[21]). The crystal orientations indicated in Fig. 3 by $\mathbf{a}\|\mathbf{B}_0$ and $\mathbf{c}\|\mathbf{B}_0$ were determined first by a direct inspection of the a- and c-rotation patterns. Confirmation of the result was achieved by fixing the orientation $\mathbf{c}\|\mathbf{B}_0$ in the low-temperature 3C phase, which can be realized on the basis of the symmetry of the structure of that phase. The latter procedure is applicable since the deviation of the monoclinic structure of the 4C phase (monoclinic angle = 89.992° according to Ref. 19) from the orthorhombic structure of the 3C phase is negligibly small if compared with the angular resolution (0.1°) in the ^{14}N NMR rotation patterns.

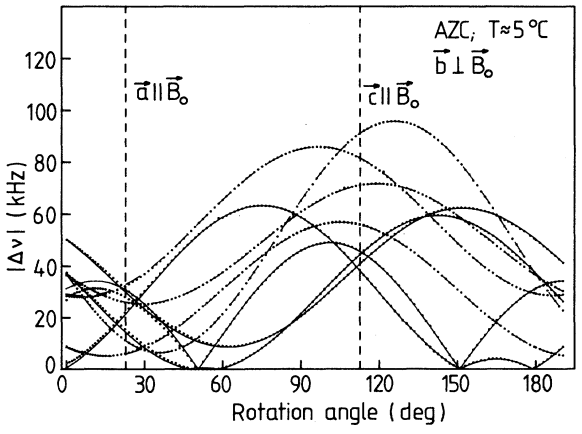

FIG. 3. Rotation pattern of the modulus of the ^{14}N NMR line splittings $|\Delta\nu|$ in the 4C phase at about 5 °C for the orientation $\mathbf{b}\perp\mathbf{B}_0$. Fit curves according to Eq. (1). Solid and dashed fit curves correspond to the N(2) and N(1) nuclei of the N phase, respectively. Compare to Fig. 1.

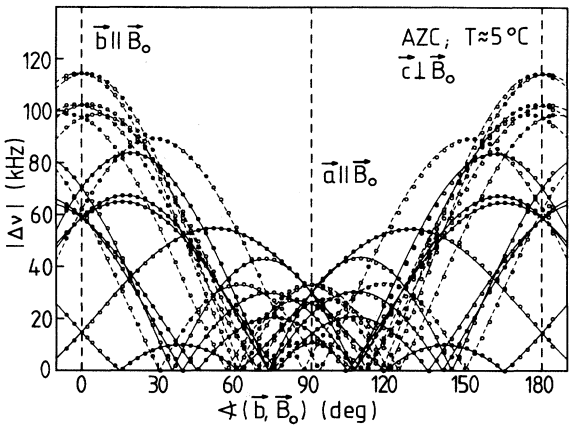

FIG. 4. Rotation pattern as in Fig. 3 for the orientation $\mathbf{c}\perp\mathbf{B}_0$. Compare to Fig. 2.

The number of resonance lines observed in Fig. 3 is by a factor of 2 smaller than expected on the basis of the space group $P1c1$ given above. A reduced number of lines is also inferred from the a- and c-rotation patterns. In the special orientations $\mathbf{b}\|\mathbf{B}_0$ and $\mathbf{a}\|\mathbf{B}_0$ (see, e.g., Fig. 4), 8 resonance lines appear which split symmetrically into 16 lines around these orientations. The mirror symmetry showing up in the splitting relative to the crystal orientations where one crystallographic direction is parallel to $\mathbf{B}_0$ is expected for the a and c rotations, on the basis of the space group proposed. The number of lines, however, is reduced in all cases by a factor of 2 if compared with the number expected from the proposed space group $P1c1$. This discrepancy can be removed, if the symmetry group $P12_1/c1$ is applied instead, which was ruled out in a previous x-ray structural analysis[19] because it led to a slightly worse R factor in the treatment of the x-ray data.

The assignment of the space group $P12_1/c1$ is, moreover, in accordance with a symmetry analysis of the phase sequence of AZC:[22] The space groups of the N and 3C phases, $Pcmn$ and $Pc2_1n$, respectively, are known to be the same as for the corresponding phases of RZB, RZC, and K_2SeO_4.[15] Thus, there is only one possible irreducible representation (Σ_2) describing the phase sequence which also particularly determines the superspace group $P^{Pcmn}_{ss\bar{1}}$ of the IC phase. Moreover, from Σ_2 one derives the possible space groups $P2_1cn$, $P1c1$, and $P12_1/c1$ for the 4C phase. Applying symmetry arguments similar to those used above in the case of the space group $P1c1$, it can be shown that the space group $P2_1cn$ is also not compatible with the ^{14}N NMR spectra in the 4C phase. Thus, only the symmetry group $P12_1/c1$ is consistent with both the symmetry properties of the ^{14}N NMR spectra reported and a symmetry analysis of the phase sequence.

All three rotation patterns performed in the 4C phase could be consistently described by the Volkoff formal-

ism[20] [Eq. (1)]. The components Φ_{ij} of the quadrupole coupling tensor at the sites of the eight inequivalent ^{14}N nuclei in the 4*C* phase could be derived. The results are summarized in Table I. The signs of the components Φ_{ii} have been chosen in such a way that the component with the largest modulus is positive. For each N site given in a row of Table I (and a one-domain sample), only one value for the off-diagonal element Φ_{xz} is admitted, the sign of which is not fixed by symmetry. This gives rise to a twofold degeneracy of the spectra. For the elements Φ_{xy} and Φ_{yz}, only those two sign combinations which differ by simultaneous changes of the signs of both elements are allowed by symmetry.

In the spectra which are the basis of the *b*-rotation pattern of the 4*C* phase, additional lines with very small intensity were detected [Fig. 5(a)] which were disregarded in the treatment until now. Their intensities changed after heating the crystal to a temperature of about 100 °C, which is about 10 °C above the phase transition to the *IC* phase. In the subsequent measurement at about 5 °C, all satellite lines possessed comparable intensities [Fig. 5(b)] and it was found that the ^{14}N NMR lines of the *b*-rotation pattern revealed mirror symmetry relative to the orientation $\mathbf{c}\|\mathbf{B}_0$. A similar increase of the number of lines could not be detected if the crystals were oriented in the magnetic field such that $\mathbf{a}\perp\mathbf{B}_0$ or $\mathbf{c}\perp\mathbf{B}_0$. The results can be ascribed to an influence of the domain structure. A direct inspection by optical methods shows, in fact,[3] that, in an originally nearly virgin one-domain crystal grown in the 4*C* phase, two different domain types taking nearly equal amounts of the sample volume can be generated by heating up the crystal to the *IC* phase and subsequently cooling down to the 4*C* phase. The domains are related to each other by the symmetry operations (c_x, n_z) missed in the *N*-*IC*-4*C* transition sequence and, consequently, are reflected in the ^{14}N NMR spectra only in the case of a *b* rotation. This also explains why no additional lines were found in the orientations $\mathbf{a}\perp\mathbf{B}_0$ and $\mathbf{c}\perp\mathbf{B}_0$. The symmetry operation c_x between the two domains, i.e., a gliding along *z* by $c/2$ of the *N* phase, is equivalent with a phase difference $2\pi/8$ for the modulation in the 4*C* phase. Consequently, at the transition from the *IC* to the 4*C* phase, in the two different domains the order-parameter modes lock in at angles φ_0 and $\varphi_0+2\pi/8$, respectively.

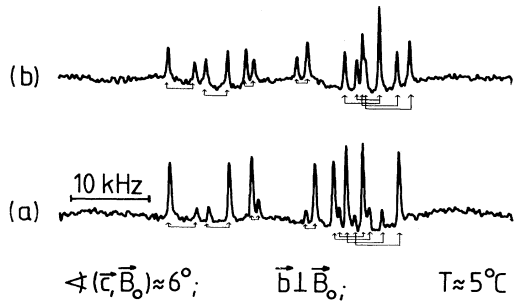

FIG. 5. Upper part of the ^{14}N NMR spectra (taken at about 5 °C) indicating the influence of the domain structure: (a) virgin crystal, (b) crystal which was stored for 2 h in the *IC* phase at about 100 °C. The lines connected by arrows differ only with respect to the sign of the tensor component Φ_{xz}. The spectra in (a) and (b) are not normalized.

The detectability of different (ferroelastic) domains of the 4*C* phase of AZC by quadrupolar perturbed ^{14}N NMR, at least in certain crystal orientations, is a special feature of the symmetry of that phase. It is well known that, on the other hand, because of symmetry, the different (ferroelectric) domains of the 3*C* phases of, e.g., AZC, RZB, and RZC principally cannot be detected by this type of NMR.

C. Crystal rotations in the incommensurate phase

In analogy with the determination of the EFG at the site of a certain nucleus for a commensurate crystal lattice and with the situation in RZB,[12] one expects that some information on the EFG at the nitrogen sites in the *IC* phase can be derived by measuring the dependence of the spectra on the crystal orientation. Because of the symmetries observed for the satellite spectra with respect to the crystal orientations where one crystal axis is parallel to $\mathbf{B}_0$, to determine the complete angular dependence it is sufficient to measure the spectra in the angular range of 90° between these definite orientations. The measurements were run at a temperature in the middle of the *IC* phase (108 °C). Following the notation used for the *N* phase, Fig. 6 shows the spectra of the upper-frequency sa-

TABLE I. EFG quadrupole coupling tensor (in kHz) at the eight inequivalent ^{14}N sites in the 4*C* phase at about 5 °C. The superscripts 1,. . .,4 indicate the four different sites belonging to each kind of *N*, defined according to the *N* phase by following the temperature dependence of the frequencies into the 4*C* phase (see text).

	Φ_{xx}	Φ_{yy}	Φ_{zz}	Φ_{yz}	Φ_{xz}	Φ_{xy}
$N^1(1)$	−32.9	114.2	−81.2	±25.1	15.3	±3.2
$N^2(1)$	−10.8	102.1	−91.2	±23.8	−19.7	±4.3
$N^3(1)$	−26.0	97.3	−71.0	±20.7	−5.1	±13.0
$N^4(1)$	−5.9	61.7	−55.8	±35.3	6.9	±51.2
$N^1(2)$	−29.9	70.5	−40.9	±27.8	−26.2	±38.9
$N^2(2)$	−21.6	59.0	−37.8	±31.5	32.5	±27.3
$N^3(2)$	−14.4	58.6	−44.4	±34.7	−25.9	±22.2
$N^4(2)$	−30.2	−14.7	45.2	±12.0	16.6	±31.4

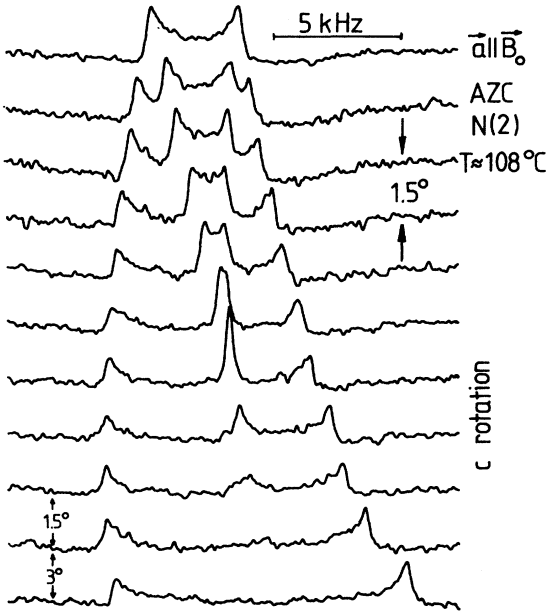

FIG. 6. Dependence of the upper frequency ^{14}N NMR satellite spectra of N(2) nuclei on the crystal orientation for a c rotation ($\mathbf{c}\perp\mathbf{B}_0$) near the crystal orientation $\mathbf{a}\|\mathbf{B}_0$ in the *IC* phase at about 108 °C. The spectra are not normalized.

tellite transition of N(2), which were detected at certain crystal orientations on rotating the crystal around $\mathbf{c}\perp\mathbf{B}_0$ away from the crystal orientation $\mathbf{a}\|\mathbf{B}_0$. For the orientation $\mathbf{a}\|\mathbf{B}_0$ there is a symmetrical frequency distribution showing the typical two edge singularities. Rotating the crystal away from this orientation, either singularity splits into two. At increasing angle, the two inner singularities move towards each other, coincide, and finally disappear in the incommensurate background spectrum at angles of rotation of about 15°. The two outermost edge singularities show a strong dependence on the crystal orientation and can be observed for all rotation angles.

The behavior of the upper-frequency satellite transition of N(2) for the same crystal rotation in the vicinity of $\mathbf{b}\|\mathbf{B}_0$ (not shown) is qualitatively the same.[21] However, on rotating the crystal apart from that orientation, the two inner singularities merge into one of the two outermost edge singularities, whereby its intensity increases. At angles of rotation of about 15°, the amplitude of this outermost singularity reduces approximately to the initial value, thus indicating the disappearance of both the inner singularities in the background. The corresponding c-rotation patterns of the singularities are presented in Figs. 7 and 8 for N(1) and N(2), respectively. In Fig. 8, and in the following, the distance between corresponding singularities of the upper- and lower-frequency distribution is denoted by first-order splitting in the *IC* phase. In Figs. 9 and 10 the corresponding a-rotation patterns of the first-order splitting in the *IC* phase are shown for N(1)and N(2) nuclei, respectively. The fit curves are based on the theory discussed in Sec. IV.

These results fulfill the general properties required by

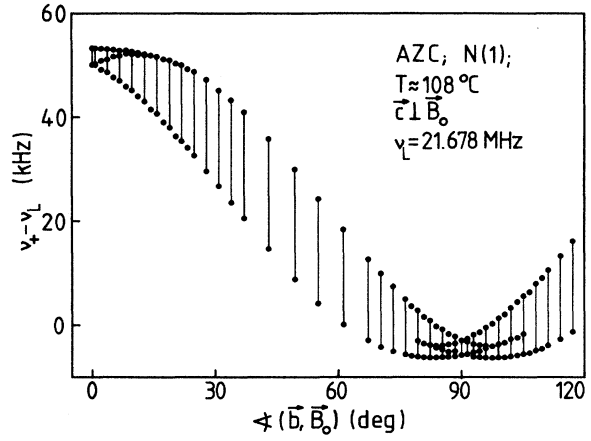

FIG. 7. Rotation pattern ($\mathbf{c}\perp\mathbf{B}_0$) of the upper part $\nu_+-\nu_L$ of the frequency distribution for N(1) nuclei in the *IC* phase at about 108 °C. $\nu_L=21.678$ MHz is the Larmor frequency. Points and lines indicate the frequencies of the singularities (mostly edge singularities) and the *IC* spectrum, respectively. Compare to Figs. 2 and 4.

symmetry[11] stating that the degeneracies and symmetries of the rotation patterns of the continuous NMR frequency distributions observed in an IC structure are the same as those of the discrete lines which the average structure would exhibit. For AZC the average structure is identical with the structure of the *N* phase. In particular, this result can be inspected directly by comparing Fig. 2 with Figs. 7 and 8. This behavior is discussed in more detail in Sec. IV.

D. Temperature dependence of ^{14}N NMR spectra for special crystal orientations

The special orientations $\mathbf{b}\|\mathbf{B}_0$ and $\mathbf{c}\|\mathbf{B}_0$ were chosen because, in the *IC* phase, the widths of the spectra are small

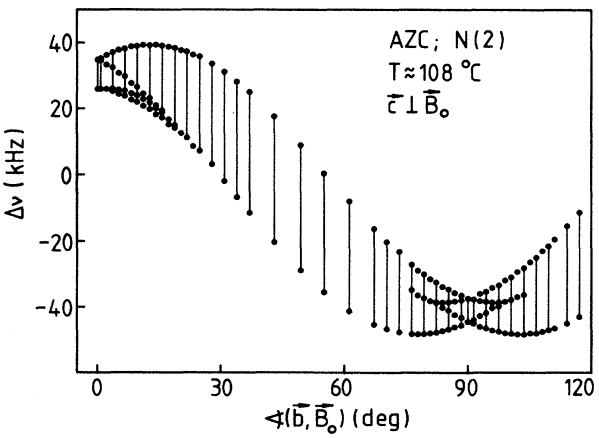

FIG. 8. Rotation pattern ($\mathbf{c}\perp\mathbf{B}_0$) of the frequency distribution of the first-order quadrupole splitting $\Delta\nu=\nu_+-\nu_-$ for N(2) nuclei in the *IC* phase at about 108 °C. Compare to Figs. 2, 4, and 7.

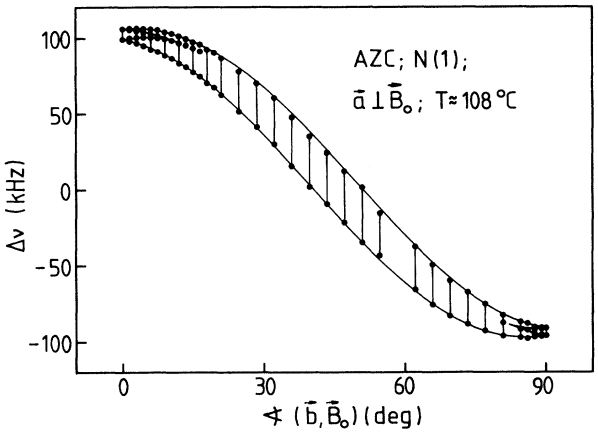

FIG. 9. Rotation pattern ($\mathbf{a} \perp \mathbf{B}_0$) of the frequency distribution of the first-order quadrupole splitting $\Delta\nu = \nu_+ - \nu_-$ for N(1) nuclei in the *IC* phase at about 108 ° C. Compare to Fig. 7.

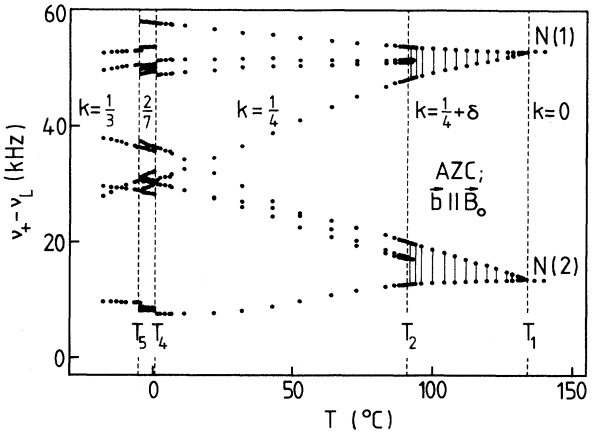

FIG. 11. Temperature dependence of the frequencies $\nu_+ - \nu_L$ in the ^{14}N NMR spectra in the orientation $\mathbf{b} \parallel \mathbf{B}_0$. In the *C* phases and the *IC* phase the frequencies are given for discrete lines and edge singularities, respectively. The Larmor frequency is $\nu_L = 21.678$ MHz.

and, consequently, an appropriate signal-to-noise ratio was achieved. Moreover, because of the strong orientational dependence of the spectra in these orientations, the correct orientation of the crystal could be easily checked and readjusted by inspecting the NMR spectra. The measurements were performed between −20 °C and about +140 °C.

In Fig. 11 the temperature dependence of the upper transition frequency $\nu_+ - \nu_L$ is shown. As already mentioned, two line pairs ascribed to N(1) and N(2) nuclei appear in the *N* phase above 135 °C in accordance with the symmetry relations of the *Pcmn* space group. Since the frequency distributions in the IC phase continuously emerge from these high-temperature lines, the notations N(1) and N(2) are also retained for the *IC* phase. Based on this temperature dependence, the assignment of the 8 and 6 line pairs in the 4*C* and 3*C* phases, respectively, to N(1)- and N(2)-type nuclei can readily be achieved. For the $\frac{7}{2}C$ phase, 14 line pairs may be identified in Fig. 11.

Since the total number of nitrogen nuclei is 56, in this commensurate phase a fourfold degeneracy may also be suggested as opposed to the triclinic structure guessed previously.[23] The spectra measured in the orientation $\mathbf{c} \parallel \mathbf{B}_0$ (Fig. 12) show essentially the same features except for the number of lines observed in the $\frac{7}{2}$C phase for which only 11 satellite pairs could be resolved. Since lines may overlap in the spectra, this reduced number of spectral components does not contradict the suggestions concerning the symmetry. Unfortunately, more detailed NMR data are not available for the $\frac{7}{2}C$ phase. Nevertheless, from the temperature dependences shown in Figs. 11 and 12, the general conclusion can be drawn that a fourfold degeneracy is maintained in the spectra through the phase sequence 4*C*-$\frac{7}{2}C$-3*C*. Moreover, it can be seen that, at T_i, anomalous temperature dependences of the NMR

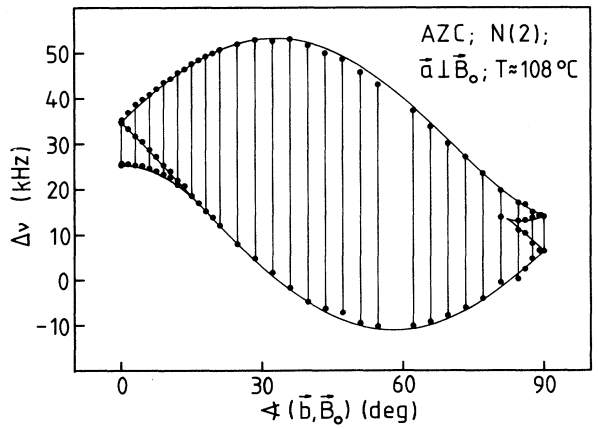

FIG. 10. Rotation pattern in the *IC* phase as in Fig. 9 but for N(2) nuclei. Compare to Fig. 7.

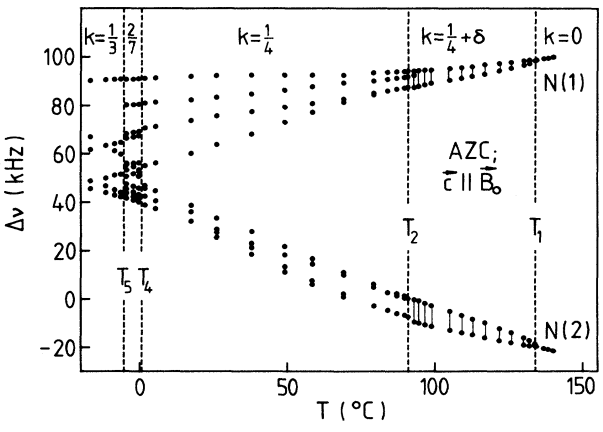

FIG. 12. Temperature dependence of the first-order quadrupole splitting $\Delta\nu$ in the ^{14}N NMR spectra in the orientation $\mathbf{c} \parallel \mathbf{B}_0$. Compare to Fig. 11.

spectra arise which can be followed through the *IC* phase and the subsequent *C* phases on passing to lower temperatures.

In a narrow temperature range of some few K above the lock-in transition at $T_c = T_2$ in the *IC* phase, certain centers of intensity (*C* lines) are detectable[21] which are precursors of the lines of the neighboring commensurate 4*C* phase. This indicates that, in this temperature range, nearly commensurate regions of sufficient extension exist which are separated by phase solitons. These effects are qualitatively similar to those which have been investigated and discussed in some detail for the lock-in transition of RZC (for more particulars see Ref. 24 and works cited within). Because of the poor signal-to-noise ratio and the narrowness of the temperature interval where the *C* lines can be observed, we make no attempts to relate our results to a quantitative variable of state like, e.g., the soliton density. The NMR measurements definitely confirm a rather big thermal hysteresis of about 5 K near T_c between heating and cooling runs which was detected for the first time by inspecting the dielectric behavior[3] and which may be related, as usual, to a pinning of the soliton lattice. From our experiments we have no direct indication to what extent we deal with an extrinsic or intrinsic effect.

The temperature dependence of the distances of the edge singularities given in Fig. 12 are presented in Fig. 13. Since the crystal was oriented with one of the crystal axes parallel to the static magnetic field, i.e., in this $\mathbf{c} \| \mathbf{B}_0$, a quadratic case was realized, for which, disregarding fluctuations, the width of the frequency distribution should be proportional to the square of the order-parameter amplitude.[13] Taking into account, however, fluctuations, the width of distribution should obey a power law proportional to $(T_i - T)^{\bar{\beta}}$, where $\bar{\beta} \neq 2\beta$ is the appropriate critical exponent[13] (see discussion below). A corresponding fit given in Fig. 13 yields $T_i = 134.5\,^{\circ}\mathrm{C}$ and $\bar{\beta} = 0.8 \pm 0.1$ for N(1), and $\bar{\beta} = 0.75 \pm 0.1$ for N(2) nuclei.

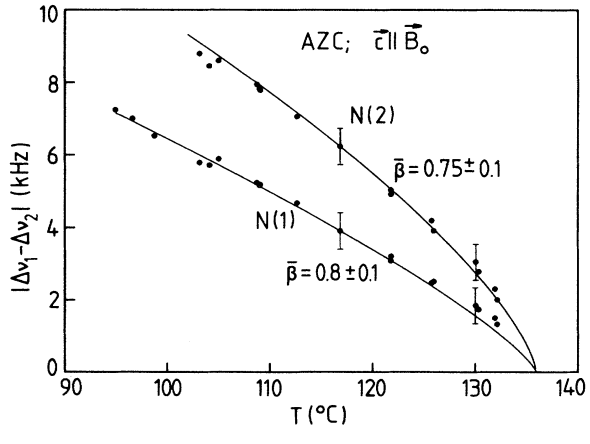

FIG. 13. Temperature dependence of the distance $|\Delta\nu_1 - \Delta\nu_2|$ of the edge singularities in the *IC* frequency distribution taken from Fig. 12 for N(1) and N(2) nuclei. The fit curves correspond to the critical exponents $\bar{\beta}$ given.

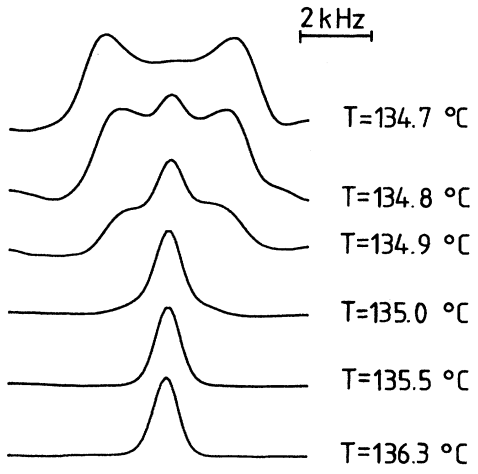

FIG. 14. Temperature dependence of the ^{14}N NMR line shape at the *N-IC* transition for N(1) nuclei [orientation $\mathbf{c} \perp \mathbf{B}_0$, $\angle(\mathbf{b}, \mathbf{B}_0) \approx 45°$] after reduction of the temperature gradient in the probe head.

Similar values can be derived from the data given in Fig. 11. Unfortunately, the accuracy of these data is not satisfactory because of the following reasons: The widths of the ^{14}N NMR frequency distributions in the *IC* phase are small for these crystal orientations. Moreover, a further source for errors is the determination of T_i. The value given somewhat differs from the more precise value 135.05 °C mentioned below. However, the critical exponents $\bar{\beta}$ determined here for AZC are comparable to the more precise values determined previously from ^{87}Rb NMR studies on RZC (Ref. 13) ($\bar{\beta} = 0.83 \pm 0.03$) and on RZB (Ref. 12) ($\bar{\beta} \approx 0.84$). For the latter, the larger widths of the satellite transition frequency distributions could be measured with higher accuracy in the same crystal orientation.

For a further and more precise study of the critical

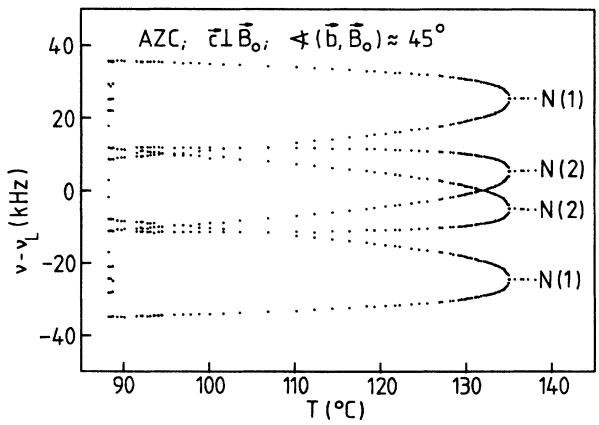

FIG. 15. Temperature dependence of the ^{14}N NMR lines and edge singularities, for N(1) and N(2) nuclei in the orientation given.

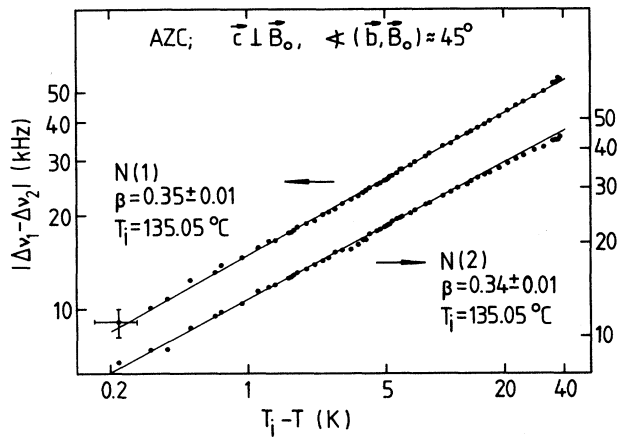

FIG. 16. Double logarithmic plot of the temperature dependence of the distance $|\Delta\nu_1-\Delta\nu_2|$ of the edge singularities in the *IC* frequency distribution taken from Fig. 15 for the determination of the critical exponent β.

effects below T_i, a crystal orientation was chosen [$\mathbf{c}\perp\mathbf{B}_0, \angle(\mathbf{b},\mathbf{B}_0)\approx 45°$] where, for the temperature dependence of the width of the frequency distribution, a term proportional to the order-parameter amplitude is dominant (linear case). A high accuracy in determining the critical behavior was achieved after reducing the temperature gradient in the NMR probe head. The high quality of the temperature regulation finally realized may be inferred from the temperature dependence of ^{14}N NMR spectra near T_i in a suitable crystal orientation (Fig. 14). The *N* and *IC* phases coexist within a temperature interval smaller than about 0.2 K contrary to the initial situation for the same probe head (coexistence region more than 1 K). From a line-shape analysis we derived the transition temperature, defined by the condition that half of the sample is in the *IC* phase, to be $T_i=(135.05\pm0.1)$ °C. The temperature dependence of the edge singularities is shown for the whole *IC* phase in Fig. 15. The width of the frequency distribution obeys a power law proportional to $(T_i-T)^{\beta}$ over a wide temperature range in the *IC* phase. The critical exponents are $\beta=0.35\pm0.01$ and 0.34 ± 0.01 for N(1) and N(2) nuclei, respectively (Fig. 16).

IV. DISCUSSION

In the following we discuss the results derived for the *IC* phase on the basis of the general arguments given previously.[11–13] The considerations are based on the periodicity of the *IC* modulation and on the symmetry of the *IC* phase. The space groups of the various phases of AZC are induced from *Pcmn* of the *N* phase. The *IC* phase of AZC is associated with the same superspace group $P^{Pcmn}_{ss\bar{1}}$ determined for the *IC* phase of K_2SeO_4 (Ref. 15) and used for RZB (Ref. 12) and RZC (Ref. 13) whose *N* and 3*C* phases are isomorphous to those of AZC. It will be shown that the assignment of this superspace group to the *IC* phase of AZC is, in fact, in accordance with the conclusions derived from the analysis of the quadrupolar perturbed NMR spectra. Since the superspace symmetry elements are the same as introduced in the analysis of the ^{87}Rb NMR spectra for RZB,[12] the fundamental relations derived there are applied in the following [cf. Eqs. (3) and (4) in Ref. 12] to the treatment of our ^{14}N NMR spectra in the *IC* phase of AZC.

A. Orientational dependences of the spectra in the *IC* phase

The EFG tensor components V^{μ}_{ij} in the crystal reference frame for any nuclei of the basic unit cell can be written as a Fourier series[11]

$$V^{\mu}_{ij}(v)=V^{\mu}_{Nij}+V^{\mu}_{0ij}+\sum_{n\geq 1}2|V^{\mu}_{nij}|\cos(nv+\psi^{\mu}_{nij}) \quad (2)$$

in the internal coordinate v which may be restricted to the interval $[0,2\pi)$. The EFG modulation tensor functions $V^{\mu}_{ij}(v)$ for different μ are related to each other by the symmetry operation of the superspace group. The condition derived [cf. Eq. (3) in Ref. 12] means that, in the Fourier series (2), only terms of even order appear for EFG components with $ij=xx$, yy, zz, xz; for EFG components with $ij=xy$, yz, which are zero in the *N* phase due to the mirror plane m_y, only odd terms exist.

According to symmetry, for the nuclei $\mu=1,2,3,4$ of N(1) or N(2), the frequency distributions in the *IC* phase show a twofold degeneracy for any crystal orientation and a fourfold degeneracy for the *a* and *c* rotations (Figs. 7–10) and for the crystal orientations $\mathbf{a},\mathbf{b},\mathbf{c}\|\mathbf{B}_0$. Thus, for the case of an *a* rotation, it is sufficient to consider only the two distributions $f^{\mu}(\nu_{\pm},\Theta_x)$ for one μ per N(1) and N(2). Hence, in what follows, μ distinguishes between the two different ^{14}N types. Referring to Figs. 9 and 10, we can state that the orientational dependences of the *IC* spectra for an *a* rotation show the symmetry with respect to crystal orientations with $\mathbf{b},\mathbf{c}\|\mathbf{B}_0$ as predicted by

$$f^{\mu}(\nu,\Theta_x)=f^{\mu}(\nu,-\Theta_x)\ , \quad (3)$$

where $\Theta_x=\angle(\mathbf{b},\mathbf{B}_0)$. An analogous relation holds for a *c* rotation.

The frequency modulation functions can be easily determined if the Fourier expansion Eq. (2) is combined with the usual formula to describe the orientational dependence of the spectra Eq. (1) and if only the nonvanishing terms of lowest order, i.e., terms up to second order, in Eq. (2) are used. The first-order splitting of the singularities in the quadrupolar perturbed NMR spectra in the case, for example, of an *a* rotation, are given by

$$\Delta\nu^{\mu}(v_s,\Theta_x)=\nu^{\mu}_{+}(v_s,\Theta_x)-\nu^{\mu}_{-}(v_s,\Theta_x)\ , \quad (4)$$

where v_s is the internal coordinate of the singularity. Then one obtains, for the frequencies $\nu_{\pm}$ of the transitions $m=\pm1\leftrightarrow m=0$,

$$\begin{aligned}2(\nu_{\pm}-\nu_L)=&\mp[U^{\mu}_{0yy}+U^{\mu}_{2yy}\cos(2v_s+\psi^{\mu}_{2yy})]\cos^2\Theta_x\\&\mp[U^{\mu}_{0zz}+U^{\mu}_{2zz}\cos(2v_s+\psi^{\mu}_{2zz})]\sin^2\Theta_x\\&\pm[U^{\mu}_{1yz}\cos(v^{\mu}_s+\psi^{\mu}_{1yz})]\sin(2\Theta_x)\ , \quad (5)\end{aligned}$$

where $U^{\mu}_{0ii}=(V^{\mu}_{Nii}+V^{\mu}_{0ii})3eQ/(2h)$ and, for

$n=1,2$, $U^{\mu}_{nij}=|V^{\mu}_{nij}|3eQ/h$.

The singularities of the frequency distribution occur for $v=v_s$ if the condition

$$\left.\frac{dv^{\mu}_{\pm}}{dv}\right|_{v=v_s}=0 \tag{6}$$

is fulfilled.

Since the internal coordinate v can be restricted to an interval of the length 2π and since the highest harmonic in Eq. (5) is of the type $\cos(2v)$, there are, at most, four real solutions v_s. This agrees with the experiment where, at most, four singularities were detected (Figs. 9 and 10). The components U^{μ}_{0zz} and U^{μ}_{2zz} can be readily evaluated with the aid of Eq. (5) if, for example, the distribution at $\Theta_x=0°$ (orientation $\mathbf{b}\|\mathbf{B}_0$) is examined in Figs. 9 and 10. For $\Theta_x=0°$ we find

$$\begin{aligned}\Delta\nu^{\mu}(\Theta_x=0°,2v_s^{\mu}+\psi^{\mu}_{2yy}=0,2\pi)&=U^{\mu}_{0yy}+U^{\mu}_{2yy}\ ,\\ \Delta\nu^{\mu}(\Theta_x=0°,2v_s^{\mu}+\psi^{\mu}_{2yy}=\pi,3\pi)&=U^{\mu}_{0yy}-U^{\mu}_{2yy}\ .\end{aligned} \tag{7}$$

Analogous expressions hold for $\Theta_x=90°$ ($\mathbf{c}\|\mathbf{B}_0$). The parameters U^{μ}_{0ii} and U^{μ}_{2ii} ($i=y,z$) are fixed immediately by experimental data for $\Theta_x=0°$, 90° according to Eq. (7), thus reducing the number of remaining parameters to be determined for all the other rotation angles Θ_x to three for either N site. The results of the fit of the experimental data are drawn in Figs. 9 and 10. Similar results were derived from the c rotations in Figs. 7 and 8. The parameters obtained are summarized in Table II.

From the orientational dependences of the ^{87}Rb NMR spectra measured in the *IC* phase of RZB, it was previously concluded[12] that the local approximation is in conflict with the experimental results. Applying the previous detailed arguments[12] to the present case, Figs. 7–10 demonstrate that the local approximation also fails to account for the ^{14}N NMR results obtained in the *IC* phase of AZC.

As Figs. 7–10 show, in the crystal orientations where one crystal axis is parallel to $\mathbf{B}_0$, two patterns of singularities are crossing. It has been shown previously[12] on the basis of the equations given above that the singularities which coincide belong to nuclei shifted with respect to each other by π along the internal coordinate v.

B. Temperature dependence

Following a recent work[13] dealing with the temperature dependence of the ^{87}Rb NMR satellite line in RZC, in this section the nonclassical critical exponents β and $\bar{\beta}$ in the *IC* phase of AZC are determined by means of our NMR data. The interpretation is based on the Fourier series Eq. (2) of the EFG tensor components. It has been shown that, near the transition temperature T_i, the amplitude $|V_1|$ of the first harmonic of the EFG modulation is proportional to the amplitude ρ of the static order parameter. Thus, its critical behavior is given by a power law with the critical exponent β,

$$|V_1|\propto\rho\propto(T_i-T)^{\beta}\ . \tag{8}$$

This is referred to as the linear case. According to Ref. 13, the amplitudes of the second Fourier components $|V_2|$ are generally not proportional to the square ρ^2 of the order-parameter amplitude. Its critical behavior is given by a power law with a critical exponent $\bar{\beta}$.

$$|V_2|\propto(T_i-T)^{\bar{\beta}}\ . \tag{9}$$

Accordingly, $\bar{\beta}\neq 2\beta$. This is referred to as the quadratic case.

Equation (8) applies to the temperature dependence in the orientation $\mathbf{c}\perp\mathbf{B}_0$ with $\angle(\mathbf{b},\mathbf{B}_0)\approx 45°$, where the frequency distance of the edge singularities is dominated by the amplitude $|V_{1xy}|$ of the first harmonic of the modulation of the corresponding EFG tensor component. The critical exponents $\beta=0.35\pm0.01$ and 0.34 ± 0.01 (Fig. 16) for N(1) and N(2) nuclei, respectively, are in agreement with the theoretical predictions of the three-dimensional XY model[25] resulting in $\beta=0.346\pm0.002$.

The situation described in Eq. (9) is present for the temperature dependence in the orientations $\mathbf{c}\|\mathbf{B}_0$ (Fig. 13) where the frequency distance of the edge singularities is proportional to the amplitude $|V_{2zz}|$ of the second harmonic of the modulation of the corresponding EFG tensor component. Although the critical exponents $\bar{\beta}=0.8\pm0.1$ and 0.75 ± 0.1 determined for N(1) and N(2) nuclei, respectively, are less accurate than the values for β given above, a difference between $\bar{\beta}$ and 2β becomes obvious similar to the situation described in Ref. 13. The theoretical value is $\bar{\beta}=0.832\pm0.021$.[13]

TABLE II. Fourier amplitudes U_{0ii} and U_{nij} (in kHz) and phase angles ψ_{nij} (in deg) of the EFG-modulation tensor functions in the *IC* phase according to Eqs. (5) and (6). The zero point of the phases was fixed by setting $\psi_{1xy}=0$. The amplitudes U_{0yy} and U_{2yy} were determined independently from a-rotation (bottom) and c-rotation (top) patterns.

N(1):	$U_{0xx}=-8.6$	$U_{2xx}=2.8$	$\psi_{2xx}=55$	$U_{1xy}=\pm21.2$
	$U_{0yy}=103.3$	$U_{2yy}=3.2$	$\psi_{2yy}=180$	$U_{1yz}=\pm18.0$
	$U_{0yy}=102.6$	$U_{2yy}=3.4$		$\psi_{1xy}=0$
	$U_{0zz}=-93.4$	$U_{2zz}=2.6$	$\psi_{2zz}=-290$	$\psi_{1yz}=-21$
N(2):	$U_{0xx}=-41.0$	$U_{2xx}=3.6$	$\psi_{2xx}=110$	$U_{1xy}=\pm19.0$
	$U_{0yy}=30.3$	$U_{2yy}=4.4$	$\psi_{2yy}=-10$	$U_{1yz}=\pm29.0$
	$U_{0yy}=30.1$	$U_{2yy}=4.7$		$\psi_{1xy}=0$
	$U_{0zz}=10.2$	$U_{2zz}=3.8$	$\psi_{2zz}=-235$	$\psi_{1yz}=-4$

Together with the previous results,[12,13] these data clearly demonstrate that AZC, RZB, and RZC show a universal nonclassical static critical behavior in their respective *IC* phases. Although, of course, fits of sufficient accuracy can be achieved for the temperature dependence of the order parameter by assuming classical Landau-type expansions of the free energy which take into account terms of sufficient high order in the order parameter, clear arguments against the applicability of such expansions are provided by our results: A Landau expansion would imply the relation $\bar{\beta}=2\beta$ to hold, which can be ruled out. Moreover, if the validity of such phenomenological expansions and the universal order-parameter temperature dependence are assumed to hold simultaneously, universal restrictions have to be imposed, which have no meaning in a phenomenological approach, on the expansion coefficients.

V. CONCLUDING REMARKS AND SUMMARY

We have shown that quadrupolar perturbed ^{14}N NMR can be applied for investigating static local effects of the various commensurate phases and the incommensurate phase of AZC in a manner similar to the well-known application of ^{87}Rb NMR to RZB and RZC. In our measurements, nonvanishing EFG tensors are generally observed. This means that the tetrahedral symmetry at the nitrogen site in the NH_4 group is distorted in spite of the fact that, as has been discussed previously in a general context,[26] there is no evidence of any distortion of the ammonium ion and that the surrounding protons undergo rapid reorientations[18,21] in the temperature range of the phase sequence investigated here. Hence, it may be concluded that the components of the EFG tensors do not at all reflect the properties of the N—H bonds in the NH_4 tetrahedra. They, rather, are to be considered as sensitive probes for the local properties of the AZC crystal.

The general formalism which was introduced recently for relating the temperature dependences of quadrupolar perturbed NMR spectra measured in certain crystal orientations in the incommensurate phase to the static critical behavior can be applied to analyze the quadrupolar perturbed ^{14}N NMR spectra of AZC, too. The critical exponents $\beta=0.35\pm0.01$ and $\bar{\beta}\approx0.8$ determined for AZC agree reasonably with the values $\beta=0.35\pm0.01$ and $\bar{\beta}=0.83\pm0.03$ obtained, for example, for RZC, and are consistent with the exponents predicted by the three-dimensional *XY* model. These data confirm that, as expected, the crystals AZC, RZB, and RZC show a universal static critical behavior in their respective incommensurate phases. This result is obviously not related to the fact that the incommensurate modulations of AZC on the one hand and of RZB and RZC on the other hand, lock in at different wave vectors at low temperatures.

Special emphasis was laid upon an accurate investigation of the NMR spectra in the vicinity of T_i using an NMR probe head with a carefully reduced temperature gradient of less than about 0.2 K over the crystal volume. Consequently, the transition region between the *N* and *IC* phases could be monitored by the disappearance of the sharp high-temperature ^{14}N NMR lines for the N(1)- and N(2)-type nuclei in the *N* phase and the appearance of the corresponding broader *IC* spectra. The fact that the transition occurred within a temperature interval of about 0.2 K suggests the attribution of the narrow temperature region where the NMR spectra coexist to a remaining small temperature gradient.

Furthermore, the temperature dependences of the widths of the *IC* spectra show no deviation from the power laws discussed above including, in particular, temperatures T close to T_i ($T_i-T\approx0.2$ K). As a consequence of both effects, it can be practically excluded that, in the *IC* phase of the AZC near T_i, a floating of the phase of the incommensurate modulation which, in some parts of the crystal may be pinned, occurs in other parts of the crystal. This would result in a more-or-less-pronounced partial motional averaging of the *IC* spectrum. This effect should cause the temperature dependences of the widths of the spectra to deviate from the intrinsic laws. On the basis of this argument, however, the universal critical behavior detected for the three substances mentioned is incomprehensible. The motional averaging may even result in an observable continuation of the line of the *N* phase into the *IC* phase. Also, this effect is, obviously, not present in our experiments. Hence, from a physical point of view, it may be concluded that we deal with crystals of rather good quality and that all relevant fluctuations in the *IC* phase are included in the critical temperature dependences. Motional-averaging effects of the type discussed were expected in Refs. 27 and 28 for the first time and excluded in Ref. 12 and 13 for RZB and RZC, respectively. In view of these arguments, the rather big thermal hysteresis observed near the lock-in transition of AZC and discussed above may reasonably be ascribed to an intrinsic crystal property. To summarize, quadrupolar perturbed NMR demonstrates that AZC, RZB, and RZC show a universal static critical behavior in their *IC* phases and that near T_i there is no indication for floating of the incommensurate modulation wave.

ACKNOWLEDGMENTS

The authors are indebted to the Deutsche Forschungsgemeinschaft for financial support and to J. M. Perez-Mato for stimulating discussions.

*Permanent address: Sektion Physik der Universität, Linnéstrasse 5, DDR-7010 Leipzig, Federal Republic of Germany.

[1]H. Matsunaga and E. Nakamura, J. Phys. Soc. Jpn. **50**, 2789 (1981).

[2]T. Sato, T. Osaka, and Y. Makita, J. Phys. Soc. Jpn. **53**, 1904 (1984).

[3]B. Müller, J. Petersson, U. Vogelgesang, and R. Walisch, Fer-

roelectrics **105**, 333 (1990).
[4]I. P. Aleksandrova, Ferroelectrics **24**, 135 (1980).
[5]I. A. Belobrova, A. K. Moskalev, N. V. Bizukina, S. V. Misul, and I. P. Aleksandrova, Solid State Commun. **33**, 1101 (1980).
[6]S. V. Misul and I. A. Belobrova, Phys. Status Solidi A **70**, K167 (1982).
[7]C. S. Sundaram and J. Ramakrishna, Curr. Sci. **50**, 1064 (1981).
[8]C. S. Sundaram, J. Ramakrishna, K. Chandrasekhar, and V. S. S. Sastry, Ferroelectrics **69**, 299 (1986).
[9]L. P. Ingman, M. Punkkinen, A. H. Vuorimäki, and E. E. Ylinen, J. Phys. C **18**, 5033 (1985).
[10]A. H. Vuorimäki, M. Punkkinen, and E. E. Ylinen, Chem. Phys. Lett. **161**, 561 (1989).
[11]J. M. Perez-Mato, R. Walisch, and J. Petersson, Phys. Rev. B **35**, 6529 (1987).
[12]R. Walisch, J. Petersson, and J. M. Perez-Mato, Phys. Rev. B **35**, 6538 (1987).
[13]R. Walisch, J. M. Perez-Mato, and J. Petersson, Phys. Rev. B **40**, 10 747 (1989).
[14]J. Dolinsek and R. Blinc, Z. Naturforsch **A41**, 265 (1986); **42**, 305 (1987).
[15]M. Iizumi, J. D. Axe, G. Shirane, and K. Shimaoka, Phys. Rev. B **15**, 4392 (1977).
[16]P. A. Meerburg, Z. Anorg. Chem. **37**, 199 (1903).
[17]E. Schneider and J. Petersson, Z. Phys. B **46**, 169 (1982).
[18]A. Trampert, Diploma thesis, University of Saarbrücken, 1989.
[19]H. Matsunaga, J. Phys. Soc. Jpn. **51**, 864 (1982).
[20]G. M. Volkoff, Can. J. Phys. **31**, 820 (1953).
[21]B. Müller, Diploma thesis, University of Saarbrücken, 1987.
[22]J. M. Perez-Mato (private communication); also see Ref. 21.
[23]K. Deguchi, H. Motegi, E. Nakamura and H. Fukunaga, Jpn. J. Appl. Phys. Suppl. **24**, 24-2, 761 (1985).
[24]J. Petersson and E. Schneider, Z. Phys. B **61**, 33 (1985).
[25]R. A. Cowley and A. D. Bruce, J. Phys. C **11**, 3577 (1978).
[26]Z. T. Lalowicz (unpublished).
[27]R. Blinc, F. Milia, B. Topic, and S. Zumer, Phys. Rev. B **28**, 4173 (1984).
[28]R. Blinc, P. Prelovsek, V. Rutar, J. Seliger, and S. Zumer, in *Incommensurate Phases in Dielectrics–1. Fundamentals,* edited by R. Blinc and A. P. Levanyuk (North-Holland, Amsterdam, 1986), p. 143.